A Low-Cost Linear Time-of-Flight Mass Spectrometer for Electrospray Propulsion Diagnostics

IEPC-2022-178

Presented at the 37th International Electric Propulsion Conference
Massachusetts Institute of Technology, Cambridge, MA USA
June 19-23, 2022

Christopher T. Lyne[1], Miron F. Liu[2], and Joshua L. Rovey[3]
University of Illinois at Urbana-Champaign, Urbana, IL, 61801, United States

Time-of-flight mass spectrometers (ToF-MS) have become an important tool for studying electrospray thrusters and quantifying their performance. This paper presents a low-cost ToF-MS suitable for thrusters operating in the pure-ion or mixed-droplet regimes. The use of electrostatic shielding and a custom amplifier design make the ToF-MS capable of resolving sub-nanoamp signals at a bandwidth in excess of 1 MHz. A case study using a capillary emitter with the propellant [Emim][Im] was used for validation by comparing the propellant mass flow rate calculated by ToF to an independently-measured mass flow rate. We found that the beam potential assumed for ToF calculations has a significant impact on calculation results (thrust and mass flow rate). Error in ToF mass flow rate was reduced to 0.5% by treating the beam potential as a function of mass-to-charge ratio (m/q) using data from the literature.

Nomenclature

$\boldsymbol{T}$	Thrust
$\boldsymbol{\dot{m}}$	Propellant mass flow rate
$\boldsymbol{t}$	Flight time
$\boldsymbol{m/q}$	Mass-to-charge ratio, inverse of specific charge
$\boldsymbol{V_B}$	Beam potential (also called acceleration potential)
$\boldsymbol{V_{RPA}}$	Retarding Potential or Stopping Potential
$\boldsymbol{V_{em}}$	Emitter potential
$\boldsymbol{\Delta E}$	Energy deficit or energy defect, $\Delta E = V_{em} - V_a$
ToF	Time-of-flight
ToF-MS	Time-of-Flight Mass Spectrometer
RPA	Retarding potential analyzer

I. Introduction

The miniaturization of electronics over the past several decades have led to a recent boom in small satellite missions and mission planning. Today, small satellites are used for a variety of tasks, including earth observation and climate science. Progress in propulsion system miniaturization has lagged behind the broader growth in the small satellite market [1], often due to difficulties in scaling down mature propulsion technologies. For example, electric propulsion technologies that rely on gas phase ionization, such as ion thrusters and Hall-effect thrusters, become less efficient when scaled down because their surface area to volume ratio increases, causing a corresponding increase in losses to the ionization chamber walls. Electrospray propulsion is an alternative type of electric propulsion that has come to the forefront of small satellite propulsion research. Electrospray thrusters are inherently easy to miniaturize and avoid the need for gas phase ionization by extracting charged particle beams directly from a liquid propellant. Despite these advantages, electrospray thrusters produce plumes with complex compositions and energy distributions, which reduce performance and have the potential to cause spacecraft contamination if not properly understood and controlled.

[1] Graduate Fellow, Department of Aerospace Engineering.
[2] Undergraduate Researcher, Department of Aerospace Engineering.
[3] Associate Professor, Department of Aerospace Engineering.

Furthermore, the low thrust produced by electrospray thrusters (typically < 1 μN per emitter) is difficult to directly measure. The need to characterize electrospray thruster plumes and quantify their propulsive performance has motivated the development of plume-based diagnostics capable of measuring the mass-to-charge (*m/q*) distribution in the plume. Paired with measurements of the plume energy distribution, these *m/q* data can be used to quantify thrust and specific impulse from plume diagnostics alone [2,3].

This paper describes a popular tool for measuring *m/q* distribution in electrospray plumes – the time-of-flight mass spectrometer (ToF-MS) – which has been used to study electrosprays for at least two decades [4,5]. Although other diagnostics for measuring *m/q* exist, time-of-flight is generally considered superior to other mass spectrometry techniques for electrosprays because species in the electrospray plume often have a wide *m/q* distribution and tend to fragment in free-flight. For example, quadrupole mass spectrometry is poorly suited because it is unable to differentiate between fragmented and unfragmented species, and it is limited to analyzing species with *m/q* values less than a few thousand amu/q [6].

Here, we discuss the design and validation of a low-cost time-of-flight mass spectrometer (ToF-MS) for electrospray propulsion diagnostics. Starting with a relatively simple design by Lozano [5], our ToF-MS makes two major improvements to address problems commonly encountered when using ToF-based electrospray diagnostics: (1) Shielding around the ToF gate and current collector has been improved to further reduce capacitive coupling between them, and (2) a custom amplifier has been built and directly connected to the ToF current collector to further minimize the effects of electromagnetic interference. After describing the ToF-MS design, we present a case study of a capillary emitter spraying the ionic liquid propellant [Emim][Im]. Using this case study, we validate our design and analysis methods by demonstrating parity between the propellant flow rate calculated from ToF data and the flow rate inferred from emitter current using robust correlations from the literature. The case study shows that our ToF-MS is capable of resolving time-of-flight signals that are under 1 nA in amplitude, allowing us to make spatially-resolved ToF measurements in the plume of single-emitter electrospray sources. Our ToF-MS is compact (<15 cm total length) yet suitable for studying electrospray sources operating in the pure ion regime [7] as well as capillary sources operating in the mixed ion-droplet regime. Through this process, we show that building and validating a high-performance ToF-MS is within the capabilities of most university labs for a budget of only $1,000 to $2,000 USD, making this ToF-MS a valuable and accessible tool for studying electrospray sources and quantifying their propulsive performance.

II. Approach

This paper describes the design, testing, and validation of a time-of-flight mass spectrometer (ToF-MS) for plume-based thrust and propellant flow rate measurements of electrospray thrusters. In this section we describe basic time-of-flight (ToF) principles, ToF-MS system design, and the validation of ToF measurements.

II.A Low-Cost, Linear Time-of-Flight Mass Spectrometer

This section gives a basic overview of the time-of-flight technique for electrospray propulsion diagnostics. Although there are many variations on this technique, our system uses one of the simplest ToF-MS designs available, called a linear time-of-flight mass spectrometer. A diagram of the ToF-MS used in this work is shown in Figure 1. The design is based on a ToF-MS used by Lozano [5].

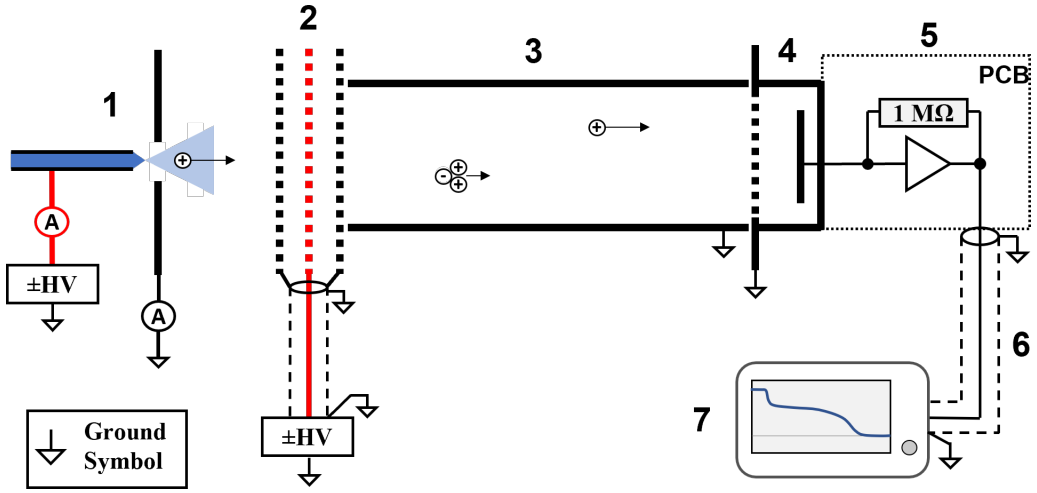

Figure 1: Time-of-Flight Mass Spectrometer (ToF-MS) system overview. (1) Electrospray source, (2) Electrostatic gate, (3) Drift tube, (4) Collector, (5) Transimpedance amplifier, (6) Coaxial cable, (7) Oscilloscope.

II.A.1 Basic Working Principles

The basic principle of time-of-flight electrospray diagnostics is to measure the time for a charged particle to travel a known distance, thereby measuring its velocity. The velocity, along with the particle kinetic energy, is used to calculate the mass-to-charge ratio of the particle. Summing over all particles in the beam, it is possible to calculate the total thrust and mass flow rate. In practice, time-of-flight data is measured as a time-dependent current signal, which can be analyzed using the equations in section II.A.2.

Consider a simple ToF-MS, as shown in Figure 1. The electrospray source sends a beam of charged particles towards the time-of-flight instrument (traveling to the right), each with a kinetic energy of qV_B. These charged particles reach the ToF collector (4 in Figure 1) at a constant rate, resulting in a constant collector current I_c. Then, at t=0 the electrostatic gate (2) is closed, blocking the beam. The charged particles that are already in the drift tube (3) when the gate is closed are unaffected and continue to move towards the collector (4). After a short time, the collector current I_c will begin to decrease, as depicted in Figure 2. The rate of change in collector current at time t is proportional to the fraction of charged particles in the beam with flight time t. For example, the step at $t = t_1$ in Figure 2 corresponds to the single ion ToF signal. The step height at $t = t_1$ gives the ion fraction for the electrospray beam. The steep drops at t_1 and t_2 indicate a narrow *m/q* distribution for ions and ion clusters, while the droplet signal (after t_2 drop) is gradual and indicates a wide *m/q* distribution for droplets. In the next section, we will see how this time-of-flight signal $I_c(t)$ can be analyzed to determine the thrust and propellant mass flow rate.

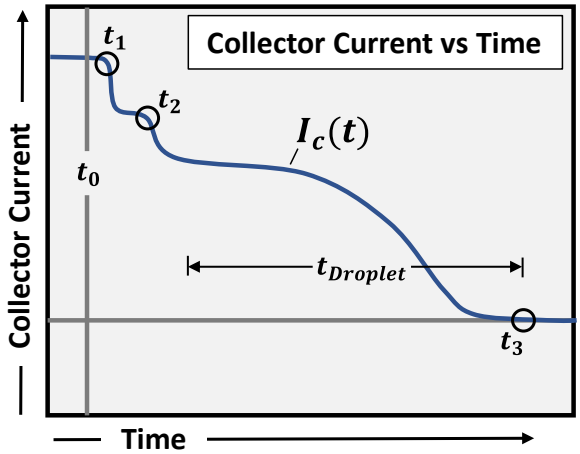

Time	Event
t_0	Gate closes to block beam
t_1	Last ion arrives at collector
t_2	Last ion cluster arrives at collector
t_3	Last droplet arrives at collector

Figure 2: Depiction of typical Time-of-Flight data (Left), in which collector current I_c is measured as a function of time. The times indicated on the plot (t_0, t_1, etc.) correspond to the events listed in the table on the right.

II.A.2 Calculating Thrust and Mass Flow Rate from Time-of-Flight Data

The time-of-flight signal consists of the time-dependent collector current $I_c(t)$ measured after gating the electrospray beam. The measured quantity is simply current as a function of time. To calculate thrust and mass flow rate from these data, we must relate flight time and mass-to-charge ratio. For a given charged particle, the flight time t is given by Eqn. 1, where L is the flight distance between the gate and collector, V_B is the beam potential (also called *acceleration potential*), and m/q is the mass-to-charge ratio. Note that the beam potential is simply the particle kinetic energy (qV_B) divided by its charge, expressed in units of eV q^{-1} or simply V.

$$t = L\sqrt{\frac{m}{2q|V_B|}} \qquad \textbf{Eqn. 1}$$

The thrust and mass flow rate can then be calculated by Eqn. 2 and Eqn. 3, respectively [4,8]. Here, I is the collector current, normalized and scaled to the magnitude of the full beam current. That is, $I = |I_B| \cdot \widetilde{I_c}$ where $\widetilde{I_c} = I_c(t) \,/\, I_{c,Gate\ Open}$. The normalized collector current $\widetilde{I_c}$ falls from $\widetilde{I_c} = 1$ at $t = 0$, to $\widetilde{I_c} = 0$ as $t \to \infty$. Thus, the derivative dI/dt is always negative regardless of the electrospray beam polarity and the gate edge (gate opening or closing). Note that dI/dt may need to be filtered to reduce noise before integrating. In this work, a Savitzky–Golay filter was applied to dI/dt before evaluating Eqn. 2 and Eqn. 3.

$$T = -\int_0^\infty \frac{2|V_B|}{L}\, t\, \frac{dI}{dt}\, dt \qquad \textbf{Eqn. 2}$$

$$\dot{m} = -\int_0^\infty \frac{2|V_B|}{L^2}\, t^2\, \frac{dI}{dt}\, dt \qquad \textbf{Eqn. 3}$$

Eqn. 1 relates mass-to-charge (m/q) to flight time (t), from which Eqn. 2 and Eqn. 3 are derived. Each of these equations requires knowledge of the beam potential V_B, which is not the same for each particle in the electrospray beam. For capillary electrospray sources, V_B can vary by more than 400 V within the beam [9,10]. Often, an 'average' beam potential is used, which attempts to represent the entire beam with a single, constant value for V_B [3]. This approach may yield reasonable results, especially for electrospray sources with low energy spread (e.g., porous and externally-wetted sources). We will see in section IV.A that, for capillary sources, treating beam potential as a function of m/q is more appropriate.

II.A.3 Data Processing for Angle-Resolved ToF

The ToF-MS used in this work samples a small portion of the full electrospray plume, corresponding to a solid angle of about 5°. By changing the position of the ToF-MS relative to the electrospray source, data can be collected at different locations in the electrospray plume. This spatially-resolved data can be used to calculate thrust and mass flow rate more accurately than full-beam ToF data [3]. In this work, ToF data were collected as a function of angle from the plume centerline. The data were processed by assuming axial symmetry and applying Eqn. 2 and Eqn. 3 according to the algorithm described in Appendix A.

II.B Time-of-Flight System Components

The time-of-flight system used in this work consists of an electrostatic gate (2 in Figure 1), a grounded metal tube (3), a collector plate (4), and a transimpedance amplifier (5). All components are stainless steel unless noted otherwise. Our ToF-MS design is based on early work by Lozano [5] with two key modifications: (1) electromagnetic shielding has been added around the time-of-flight gate and collector (Figure 3 Left), and (2) a custom transimpedance amplifier has been built and directly mounted to the collector (Figure 3 Right).

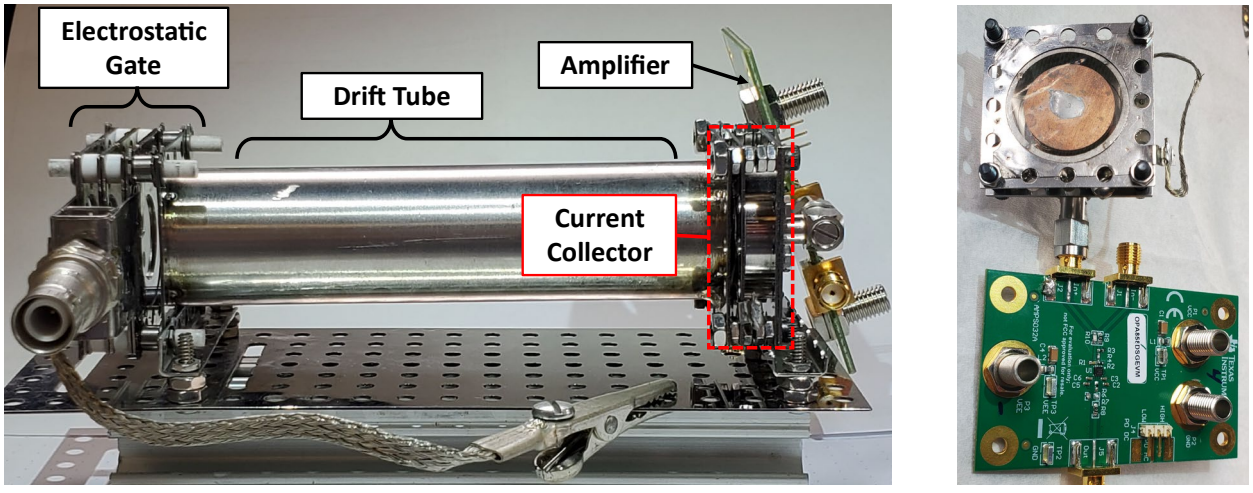

Figure 3: (Left) Time-of-Flight Diagnostic used in this work. The gate and collector are both surrounded by electromagnetic shielding and use shielded coaxial cables. (Right) Current collector coupled to transimpedance amplifier.

Our time-of-flight system was constructed mostly from Kimball Physics eV Parts. Some components were permanently joined using an inexpensive, battery powered spot welder.

II.B.1 Electrostatic Gate

The electrostatic gate consists of three square plates with 0.625" (15.9 mm) apertures covered by a 90.1 lpi mesh with 88% transparency (MN20, Precision Eforming LLC.) and a distance of 0.1" (2.5 mm) between plates. The outer

plates are grounded, while the plate in the center can be quickly switched between ground and high voltage. When the center plate is at ground potential, the gate is said to be 'open' and the electrospray beam can pass through the gate and into the drift tube. When the center plate is raised to high voltage, the beam is blocked, and the gate is said to be 'closed'. See section II.C.2 for more detail about the ToF gate.

II.B.2 Gate Electronics

Gate voltage is controlled by a fast switch (BEHLKE 91-01-HB-C) that switches between ground and high voltage. It is a double pole, single throw switch that provides fast switching times when opening or closing the gate. The switch is capable of handling high voltage in either polarity, so ToF data can be collected for electrospray sources operating in positive or negative emission mode. High voltage for the positive and negative polarities are provided by DC-DC converters so that the entire high-voltage circuit can be contained within a grounded aluminum box. Ultra-fast, high-voltage Schottky diodes were used to prevent reverse current at the switch poles to protect the switch from oscillations in the load circuit. Voltages at the switch poles were buffered with 5 nF, ±10 kV ceramic capacitors. Peak current through the switch was limited by a resistor in series with the load (470 Ω, OHMITE TFS series), which resulted in a gate voltage rise time of about 300 ns. The switch control signal was provided by a signal generator (Siglent SDG1032X) via a 5 V square wave. A capacitive voltage divider with ~1000x attenuation provided the oscilloscope trigger for ToF data acquisition. We found that the trigger event could be more reliably detected by limiting the oscilloscope bandwidth to 20 MHz and lowpass filtering the trigger signal to around 7 MHz. Consistent triggering is especially important if waveform averaging will be used.

II.B.3 Drift Tube

The drift tube consists of a straight metal tube that is grounded. The region inside the tube is shielded from external electric fields, allowing charged particles to drift without changing velocity. The drift tube has a square plate with a central aperture welded onto each end to allow the electrostatic gate and the ToF collector to be easily attached to the tube.

II.B.4 Collector

The current collector consists of a 0.75" (19 mm) copper disc (i.e., the collector plate) that measures the current associated with charged particles reaching it. The collector plate is surrounded by a grounded shell that acts as a faraday cage, blocking external electric fields and electromagnetic noise from reaching it. The entrance to the collector is covered by grounded mesh (90.1 lpi, 88% transparency) that allows charged particles to pass into the collector from the drift tube. The collector is electrically connected to the amplifier by an SMA coaxial connector (Hirose HRM-405S(40)). See section II.C.2 for more detail about the ToF collector.

II.B.5 Transimpedance Amplifier

The transimpedance amplifier (TIA) is an electronic circuit that is used to measure current, typically when a fast time response (high bandwidth) is required. Commercial-off-the-shelf (COTS) TIAs are available, such as the DHPCA-100 by FEMTO, which provide low-noise current measurements suitable for a variety of applications, including time-of-flight diagnostics. For this work, we chose to fabricate a custom TIA using the OPA858 operational amplifier (op-amp) from Texas Instruments. The TIA was fabricated starting from an 'evaluation module' (Texas Instruments OPA858EVM) by replacing a small number of components. The TIA has a transimpedance gain of 10^6 Ω and maximum bandwidth of about 10 MHz. This custom TIA was capable of measuring sub-nanoamp signals at 1.4 MHz bandwidth by using waveform averaging to increase signal-to-noise ratio.

We found the performance of the TIA was sufficient for our application. Here, we used it for spatially-resolved *m/q* measurements in the plume of a single capillary emitter. Spatial resolution in ToF data enable thrust and mass flow rate to be quantified more accurately [3] and allow the structure of the electrospray plume to be studied in detail. Comparing the custom TIA with a COTS option (DHPCA-100), the COTS amplifier has a noise level about 2.4 times lower than our TIA when measured at ~1 MHz. However, we found the custom TIA performance was sufficient for our application and offers significant cost savings over the COTS option (~$150 vs. ~$3k to $4k USD).

Appendix B discusses the design, fabrication, and performance of the custom transimpedance amplifier (TIA) used in this work.

II.C Signal-to-Noise Optimization for Time-of-Flight

A common challenge encountered when building time-of-flight diagnostics for electrospray applications is the relatively low signal levels (i.e., small collector current) coupled with the need for high-speed operation and, consequently, noise. This section describes techniques used to improve the overall signal-to-noise ratio for ToF measurements.

II.C.1 Maximizing signal-to-noise ratio

The small signals and fast time scales associated with time-of-flight electrospray diagnostics present a challenging

combination. Often, a settling time on the order of 100s of nanoseconds is required, equivalent to an amplifier bandwidth of about 1 to 5 MHz. Noise typically scales with the square root of bandwidth, making fast amplifiers inherently noisy. A useful figure of merit is the signal-to-noise ratio (S/N), which should be as high as possible while meeting other design criteria, such as minimum bandwidth. Appendix B discusses transimpedance amplifier design, including ways to maximize S/N. A basic conclusion of that discussion is that the signal-to-noise ratio for a transimpedance amplifier is roughly proportional to the square root of the feedback resistance, as shown in Eqn. 4. Consequently, the largest possible value of R_F should be used that meets the required application bandwidth and does not destabilize the amplifier.

$$\frac{S}{N} \sim \sqrt{R_F} \qquad \textbf{Eqn. 4}$$

After optimizing the amplifier design, the signal-to-noise ratio can be further increased by increasing the signal amplitude or decreasing the noise associated with the measurement. We will discuss both strategies in the following paragraphs.

Increasing Signal Strength

Perhaps the simplest route to increase the signal-to-noise ratio is by increasing the signal strength (i.e., increasing the collector current). A common approach is to use large-area collectors that sample most of electrospray plume simultaneously [9,11]. Although this approach maximizes the ToF signal strength, flat large-area collectors tend to distort *m/q* measurements because the flight length depends on angle from the plume centerline, $L_{tof} \sim 1/\cos(\theta)$. As noted by others, a rigorous approach to measuring the thrust and mass flow rate from electrospray plume data requires spatially-resolved measurements, which cannot be made using a large-area collector [3].

Another common approach to increase ToF signal strength is to use electrostatic lenses to focus the electrospray plume, increasing the fraction of beam current that reaches the collector [5,12]. However, simple electrostatic focusing is not suitable for electrospray sources with a broad kinetic energy distribution, such as capillary electrosprays [5].

Given that focusing the electrospray plume is not always feasible, and that a large-area collector is not able to make spatially-resolved measurements, we can consider two remaining options to increase ToF signal strength: (1) produce a higher beam current, or (2) replace the collector plate with a detector that actively gains the signal such as an electron multiplier or a microchannel plate (MCP).

Reducing Random Noise

Another strategy to increase the signal-to-noise ratio is by decreasing random noise. Here, the two primary sources of random noise are electronic noise (i.e., Johnson noise) and noise due to electromagnetic interference. Electronic noise can be minimized through proper amplifier design, which is discussed in Appendix B. In our design, electromagnetic interference was reduced using grounded shielding, and by minimizing the distance between the collector and transimpedance amplifier (see section II.C.2).

Besides optimizing the time-of-flight instrument design, we used two main strategies to reduce random noise in our measurements. The first is using the minimum measurement bandwidth that satisfies our response time requirements. Although the transimpedance amplifier used in this work has a bandwidth of about 10 MHz, the oscilloscope used is capable of low-pass filtering the signal to limit the measurement bandwidth. Since most noise scales with $\sqrt{f}$ where f is the measurement bandwidth, low-pass filtering to the minimum required bandwidth improves S/N. The second technique applied here is waveform averaging, in which n time-of-flight waveforms are averaged together to increase S/N by a factor of $\sqrt{n}$.

II.C.2 Reducing gate-induced noise

For time-of-flight systems using an electrostatic gate, capacitive coupling between the gate and the collector is often the single largest source of noise interfering with the ToF signal. If the coupling between the gate and the collector is not sufficiently reduced, the noise induced by the gate on the collector can easily obscure the time-of-flight signal. This capacitive coupling can be reduced by placing conductive shielding between the gate and collector, as shown in Figure 4. High voltage is carried to the gate (Figure 4, left) via a shielded coaxial cable. The cable connects to an SHV jack (1), which is mounted to a bracket that is spot welded to the grounded outer plates (4). The center conductor of the SHV jack is soldered to the gate electrode (2, 3). By attaching a coaxial connector directly to the gate, we are able to use a shielded coaxial cable for the entire length of cable leading to the gate. This significantly reduces gate-induced noise compared to using unshielded cable for part or all of the gate cabling.

Shielding on the collector (Figure 4, right) consists of a grounded housing around the collector plate. The electrospray beam travels through a mesh-covered aperture at the collector entrance (1). Charged particles impact the collector plate (3), which is soldered to the center conductor of an SMA coaxial connector (4). In our design, the transimpedance amplifier is directly connected to the SMA jack, inside the vacuum chamber. This direct connection has

two main benefits. The first is that capacitive coupling to the gate, and therefore noise, is significantly reduced by the minimal distance between the collector and amplifier and by the high-quality shielding provided by the rigid coaxial connector. The second benefit is that the total capacitance connected to the amplifier input is minimized. This allows for a higher amplifier bandwidth (faster response time), as discussed in Appendix B, which improves the *m/q* resolution of the ToF-MS.

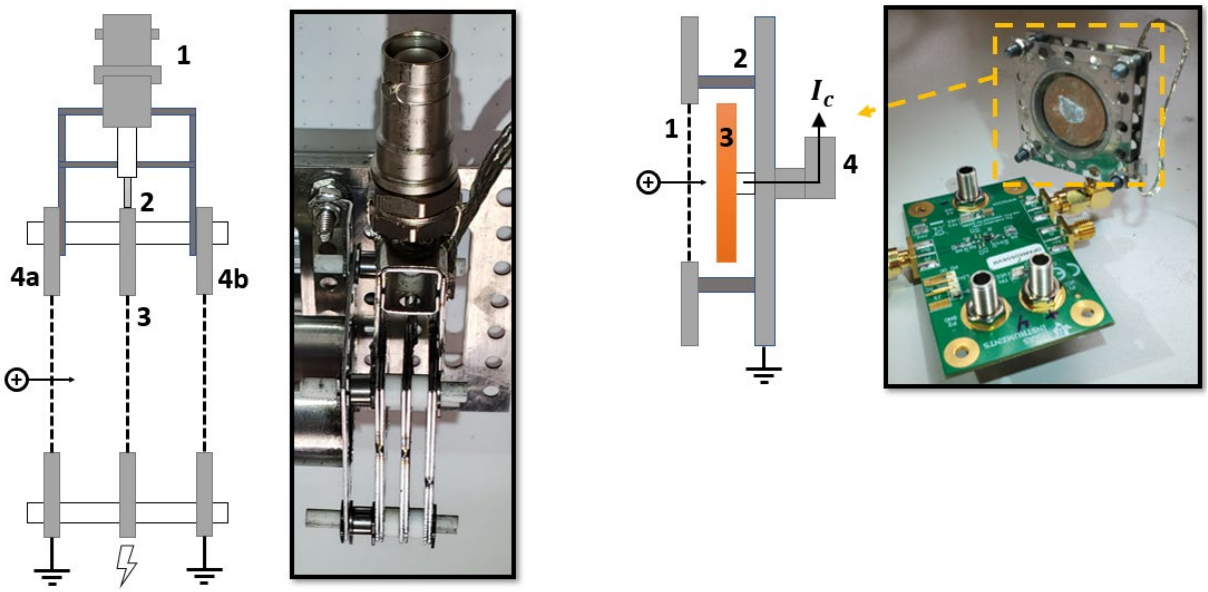

Figure 4: Gate (left) and collector (right) with shielding to reduce capacitive coupling between them. 'Flying ion' shows path of electrospray beam.

Gate (Left): (1) SHV connector, (2) SHV center conductor soldered to middle plate, (3) High-voltage plate and mesh-covered aperture, (4a) and (4b) grounded outer plates.

Collector (Right): (1) Grounded front plate and mesh-covered aperture, (2) Grounded tube and rear plate, (3) collector plate (copper disc), (4) SMA connector

In summary, our main suggestions for reducing gate-induced noise are:

1. Surround the collector and gate with grounded shells (shielding) to reduce capacitive coupling between them.
2. Use shielded cables for the gate voltage and collector current.
3. Minimize the length of cable between the collector and the ToF signal amplifier.
4. Make high-quality ground connections, preferably using conductors with high surface area such as braid.

Compared to Lozano's design (2003) [5], our ToF-MS is considerably more compact ($L_{ToF} = 116\,mm$ vs. $746\,mm$) yet the gate-induced noise has a similar amplitude to Lozano's system (~4 nA peak vs. ~2nA peak). Furthermore, the duration of the gate-induced noise is considerably shorter for our system (260 ns FWHM vs. ~4 µs FWHM). The flight time of the fastest ions is about 1.5 – 2 µs for our system, so by the time the ion signal arrives ($t \approx 1.5 - 2\,\mu s$) the gate-induced noise has settled and does not negatively affect the ToF measurements.

II.D Time-of-Flight System Validation: Capillary Emitter Case Study

As described in section II.A.2 and Appendix A, time-of-flight data can be used to obtain indirect thrust and mass flow rate measurements for electrospray thrusters. In order to validate our time-of-flight instrument and data analysis methods, we take measurements in the plume of a capillary electrospray source. For capillary electrosprays, the source emitter current is related to the propellant flow rate by well-established correlations, thus providing a measure of propellant flow rate that is independent from time-of-flight data. This reference flow rate, $\dot{m}_{Ref}$, is then compared to the mass flow rate calculated using time-of-flight data, $\dot{m}_{ToF}$, to assess the accuracy of our time-of-flight measurements and methodology.

Capillary electrosprays of [Emim][Im] have been extensively studied, for example by Gamero-Castaño [3,4,9,11] and Miller [6,10]. Among these literature data is the emitter current I_{em} as a function of propellant volumetric flow rate Q (leftmost two columns of Table 1 in [11]), which follows the scaling laws described by Gañán-Calvo [13]. The robust relationship between I_{em} and Q allow the flow rate to be determined from the source emitter current, which is

considerably simpler than making direct measurements of propellant flow rate, for example, by using a bubble flow meter [4,11]. The results of our validation study are presented in section III.

II.D.1 Electrospray Source Description

The capillary electrospray source used for time-of-flight validation was a stainless steel emitter with an inner diameter of 50 µm and an outer diameter of 360 µm (New Objective, Inc.) spaced approximately 1 mm from an extractor with an aperture of 1.6 mm. The extractor was grounded, and 2 kV was applied to the emitter. The emitter polarity was alternated to prevent electrochemical degradation of the propellant, but time-of-flight data were only collected in positive charge emission mode (cation mode). Propellant was fed to the emitter using fused silica tubing with an inner diameter of 150 µm and an approximate length of 1 m.

III. Results

Time-of-flight data were acquired for a capillary electrospray source spraying the ionic liquid [Emim][Im]. ToF data were collected as a function of angle from the plume centerline, yielding spatially-resolved *m/q* distributions in the plume. These data were analyzed using the method described in Appendix A, yielding the total thrust (T) and propellant mass flow rate ($\dot{m}_{ToF}$). The mass flow rate was then compared against an independent measure of propellant mass flow rate, $\dot{m}_{Ref}$, to validate our time-of-flight instrument and methodology. The following sections present the results of that validation study.

III.A Time-of-Flight Data

Figure 5 shows the raw time-of-flight signal in response to the electrostatic gate opening at $t = 0$. For a review of the regions of the time-of-flight curve and how they can be interpreted, refer to Figure 2. The anomalous signal near $t = 0$ is caused by the gate, rather than by the electrospray plume. The center of the plume, defined as the angle at which the maximum plume current density was measured, was found to be about 5° offset from the geometric centerline of the electrospray source, probably due to misalignment between the emitter and extractor. In our data analysis, the angles shown are relative to the centerline of the plume rather than the geometric center of the electrospray source.

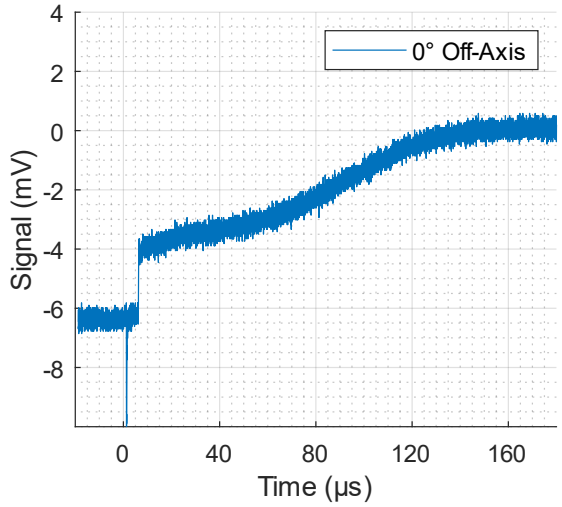

Figure 5: Signal output from the transimpedance amplifier measuring a +6 nA collector current ($n = 256$), y-shifted so that the current at late time is taken as a zero reference. At $t = 0$, the gate is opened and I_c rises from zero to +6 nA (+6 mV signal). The peak near $t = 0$ is gate-induced noise. The step in I_c around $t \approx 5\ \mu s$ is due to low *m/q* species (ions and ion clusters), while the gradual change in I_c from $t \approx 10\ \mu s$ to $t \approx 160\ \mu s$ is due to high *m/q* species (droplets). See Figure 2 for an explanation of how to interpret ToF plots like those in Figure 5 and Figure 6.

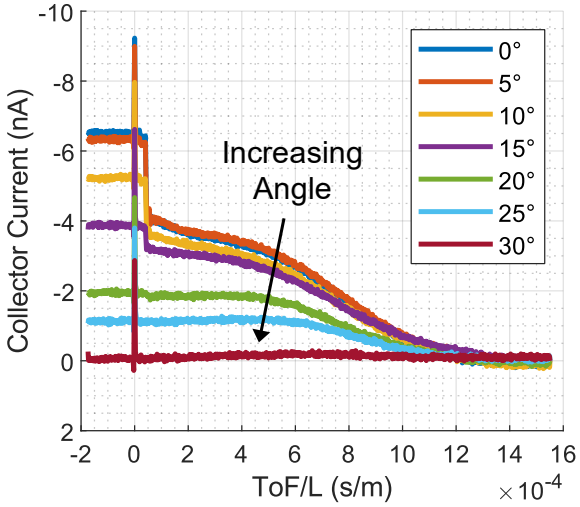

Figure 6: Collector current measured at varying angles from the center axis of the electrospray beam with a total beam current of $I_B = 485\ nA$. The plume half-angle is approximately 30°. The center portion of the beam ($\theta \approx 0°\ to\ 15°$) is comprised of a low m/q population (indicated by the step in I_c at early time) and a high m/q population (indicated by the gradual decrease in I_c from about 1 to 14 *10^{-4} S/m), which disappears at high angles ($\theta \geq 20°$)

Time-of-flight data at several angles from the plume centerline are shown in Figure 6. Note that these data are for a positive electrospray beam (positive collector current) with the electrostatic gate transitioning from closed to open. The current measured in late time ($I_C|_{t\to\infty}$) is used as the zero reference. Thrust and mass flow rate are calculated using the normalized collector current scaled to the magnitude of the beam current, which guarantees that Eqn. 2 and Eqn. 3 return positive results regardless of electrospray polarity and gate edge (opening or closing). Figure 6 also shows that there is a significant low-*m/q* population in the beam centerline ($\theta < \sim 20°$), presumably made up of molecular ions and ion clusters, as indicated by the step in I_c at early time (around $0.5x10^{-4}$ S/m). The steepness of the step indicates that the low-*m/q* population has a narrow *m/q* distribution compared to the droplet signal, which is more gradual and indicates a large spread in *m/q*.

Thrust and mass flow rate can be calculated from the time-of-flight signal (I_c) and the energy distribution in the beam (V_B). To use Eqn. 2 and Eqn. 3, the beam potential V_B must be written as a function of t. The most straightforward method of evaluating Eqn. 2 and Eqn. 3 uses an average V_B to represent the entire beam, $V_B = \overline{V_B}$, which is constant with time. We can estimate $\overline{V_B}$ from retarding potential data in the literature for comparable electrospray sources. To account for the different emitter potentials used in different experiments, we will compute the energy deficit (ΔE) from literature data and apply those results to our analysis. Energy deficit is simply an expression of energy loss ($V_B = V_{em} - \Delta E$), which remains roughly constant for a given propellant and beam current regardless of emitter potential [11].

Consulting the literature (Gamero-Castaño, 2008, figure 14), we find that the energy deficit for a 560 nA [Emim][Im] capillary electrospray is approximately 230 V for droplets and 530 V for ions. These data show reasonable agreement with the energy deficits measured by our group at the University of Illinois for capillary electrosprays of [Emim][Im] (294 V for droplets, 550 V for ions), though our data were taken at higher beam currents which generally result in higher energy deficits [14]. The mass flow rate and thrust are dominated by high-*m/q* particles (i.e., droplets), so we will assume that an appropriate average beam potential $\overline{V_B}$ is approximately equal to the average droplet potential for the purposes of calculating thrust and mass flow rate. Applying this approach with $\Delta E = 230\,V$, we find that our average beam potential is approximately $V_B = V_{em} - \Delta E = 2000\,V - 230\,V = 1770\,V$. Using the algorithm described in Appendix A with $V_B = 1770\,V$, we find that the thrust and propellant mass flow rate as measured by time-of-flight are 1.08 μN and $9.93x10^{-10}$ kg/s (0.653 nL/s), respectively.

For a more detailed discussion of beam potential V_B and its effect on thrust and mass flow rate calculations, refer to section IV.A.

III.B Time-of-Flight Validation: Comparison of Mass Flow Rates

To validate our time-of-flight results, the propellant mass flow rate obtained from time-of-flight data was compared to the flow rate determined from the emitter current using $I_{em} = f(Q)$ correlations from the literature. Table 1 summarizes the results of this comparison.

Gamero-Castaño (2008) studied capillary electrosprays of [Emim][Im] and found a robust correlation between emitter current and propellant flow rate that agrees with electrospray scaling laws [11,13]. Linearly interpolating this data to match our beam current (485 nA) yields a volumetric flow rate of $Q_{Ref} = 0.73\ nL/s$. Multiplying by the fluid density, we find that $\dot{m}_{Ref} = 1.11x10^{-9}\ kg/s = 1.11\ \mu g/s$.

Our time-of-flight data were analyzed using the angle-resolved time-of-flight equations described in Appendix A with $V_B = 1770\ V$ and $L = 116\ mm$. With these assumptions, we find that our time-of-flight measurement underestimates the mass flow rate by about 10% compared to the flow rate inferred from the emitter current. We believe that the main reason for this discrepancy is using a constant value of V_B in Eqn. 2 and Eqn. 3, despite the large energy spread typical of capillary electrospray beams. In section IV.A, we will see that better agreement between $\dot{m}_{ToF}$ and $\dot{m}_{Ref}$ is found by using a more realistic beam potential V_B for time-of-flight calculations. In future work, we plan to perform this validation for additional flow rates so that the ToF-measured mass flow rate can be validated more robustly. The validation presented here only uses a single flow rate for comparison, so it is unclear how the ToF-based flow rate measurements will perform at other operating points. Additionally, it may be beneficial to take direct flow rate measurements, using a bubble flow meter for example, to lend greater confidence in the reference flow rate used for comparison to ToF data.

Table 1: Comparison between propellant mass flow rate determined by emitter current and by time-of-flight. Summary of time-of-flight calculation results (mass flow rate, thrust, and specific impulse). Calculations assume $V_B = 1770\ V$ ($\Delta E = 230\ V$).

Flow Rate from Emitter Current	
Emitter Current	485 nA
Volumetric Flow Rate Q_{Ref} (From $I_{em} = f(Q)$, [11])	0.734 nL/s
Mass Flow Rate $\dot{m}_{Ref}$	1.11 µg/s
Time-of-Flight Results	
Mass Flow Rate	0.993 µg/s
Volumetric Flow Rate Q_{ToF}	0.653 nL/s
Thrust	1.08 µN
Specific Impulse **Using $\dot{m}_{Ref}$** **Using $\dot{m}_{ToF}$**	 99 s 111 s
Error in $\dot{m}$	
$\frac{\dot{m}_{ToF} - \dot{m}_{Ref}}{\dot{m}_{Ref}}$	**-10.5%**

IV. Discussion

IV.A The Effect of Beam Potential V_B

The thrust and mass flow rate are calculated from time-of-flight data using Eqn. 2 and Eqn. 3, repeated below, which depend on the beam potential V_B as well as the normalized, scaled collector current $I(t)$ and the flight length L.

$$T = -\int_0^\infty \frac{2|V_B|}{L}\, t\, \frac{dI}{dt}\, dt \qquad \textbf{Eqn. 2}$$

$$\dot{m} = -\int_0^\infty \frac{2|V_B|}{L^2}\, t^2\, \frac{dI}{dt}\, dt \qquad \textbf{Eqn. 3}$$

As discussed in section II.A.2, V_B is not the same for every particle in the electrospray beam. For capillary electrosprays, Miller et al. (2021) and Gamero-Castaño et al. (2021) found linear correlations between beam potential V_B (also called *acceleration potential*) and mass-to-charge ratio m/q [9,10]. Expressing their V_B data in terms of an energy deficit $\Delta E = V_{em} - V_B$, we can apply their correlations to the analysis of our time-of-flight data.

IV.A.1 Gamero-Castaño et al., 2021

Gamero-Castaño et al. studied capillary electrosprays of [Emim][Im] using a retarding potential analyzer (RPA) in

tandem with time-of-flight [9]. The RPA consisted of an electrostatic mirror that redirected charged particles into the time-of-flight instrument. The trajectory of charged particles through the mirror depends on their kinetic energy per charge (i.e., V_B), so only particles within a narrow energy band ($V_B \approx V_{RPA}$) reach the time-of-flight collector. For each value of stopping potential, V_{RPA}, they measured the m/q distribution and calculated the average m/q value. They fitted these data to obtain V_B as a function of average m/q. For [Emim][Im] at a beam current of $I_B = 450\ nA$ and 21° C, their data show that the energy deficit follows the trend $\Delta E = -9.33x10^4(m/q) + 416$ where m/q is in kg/C and ΔE is in volts.

IV.A.2 Miller et al., 2021

Using an orthogonal-extraction time-of-flight instrument, Miller et al. studied capillary electrosprays of four liquids, including [Emim][Im] [10]. Like the tandem RPA and ToF used by Gamero-Castaño et al., orthogonal ToF allows the m/q distribution to be measured for a narrow band of particle energies near V_{RPA}. That is, only charged particles with $V_B \approx V_{RPA}$ are able to reach the time-of-flight detector. They measured m/q distributions as a function of V_{RPA}, fitting the high-m/q portion of each with a log-normal distribution. From these fitted m/q data they calculated the most probable m/q for each V_B. Their data for [Emim][Im] at 0.40 nL/s suggest that the energy deficit ΔE follows the linear trend $\Delta E = -1.11x10^5(m/q) + 346$ where m/q is in kg/C and ΔE is in volts.

IV.A.3 Effect of V_B on Thrust and Mass Flow Rate Measurements

Figure 7 shows the beam potentials determined from the energy deficit fits from Miller et al. (2021) and Gamero-Castaño et al. (2021) for the emitter potential used in this work, $V_{em} = 2000\ V$. The dashed lines indicate constant beam potential, while fits of experimental data are shown in solid lines. The experimental data clearly show a trend of V_B increasing with *m/q*, suggesting that the $V_B = constant$ lines are poor fits for the plume energy distribution. To use the fits in Figure 7 to calculate thrust and mass flow rate (Eqn. 2 and Eqn. 3), the beam potential must be expressed as a function of flight time $V_B(t)$.

The change of variables can be accomplished with the following method: Start with an array of m/q values. For each m/q, use Eqn. 1 with $V_B = V_B(m/q)$ to calculate the flight time t. For each pair of m/q and its associated flight time t, set $V_B(t) = V_B(m/q)$. Now the beam potential expressed as a function of flight time, $V_B(t)$, can be directly used in Eqn. 2 and Eqn. 3.

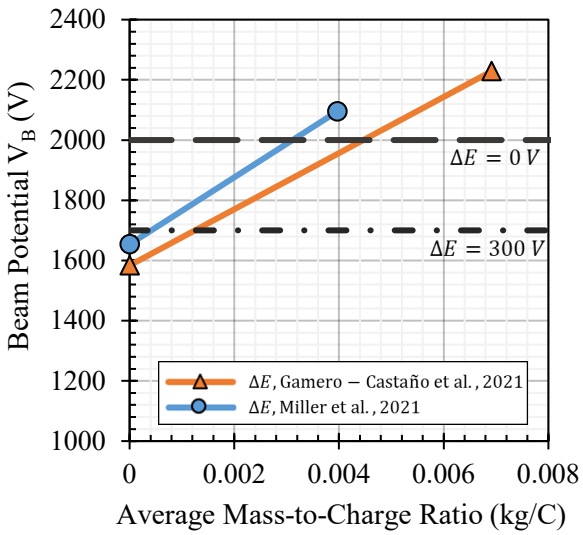

Figure 7: Beam potential V_B as a function of average m/q for $V_{em} = 2000\ V$. Dashed lines represent constant ΔE, where a constant V_a is assumed for all particles in the beam.

Both experimental fits for V_B indicate that the highest *m/q* particles reach a beam potential higher than the emitter potential. Plainly, the assertion that high m/q particles in the beam are able to reach energies larger than qV_{em} (potentials higher than V_{em}) should be viewed with suspicion. A possible explanation for these findings is that droplets traveling between the electrospray source and the RPA lose charge by ion evaporation, making their kinetic energy per charge (V_{RPA}) larger. Nonetheless, the velocity of the droplet (and evaporated ion, for that matter) has not significantly changed, and is given by conservation of energy $(1/2)mv^2 = qV_B$ where m and q are the original droplet mass and charge, respectively, and v is the droplet velocity. Since the droplet velocity does not appreciably change when an ion evaporates from its surface, the droplet's flight time also does not change significantly. Therefore, assuming that the stopping potential V_{RPA} is equal to the beam potential V_B may lead to an overestimate of beam potential. Despite this, the time-of-flight data obtained using these experimental fits for V_B appear to be quite accurate.

Table 2 shows the thrust and mass flow rate calculated using Eqn. 2 and Eqn. 3 for various assumed beam potentials. For the case where V_B is constant, the calculated thrust and mass flow rate are linearly proportional to V_B. If V_B as a function of m/q is not known, RPA data can be used to estimate upper and lower bounds on V_B and those bounds can be used to calculate bounds on T and $\dot{m}$. The results in Table 2 indicate that the best match between the mass flow rate calculated from emitter current and that measured by time-of-flight is obtained when the beam potential is assumed to be a function of *m/q*, $V_B = V_B(m/q)$. We find that of the mass flow rate calculated from time-of-flight data differs from that inferred from emitter current ($\dot{m}_{Ref}$) by -0.5% using the Gamero-Castaño et al. (2021) fit for $V_B(m/q)$ and by +8.9% using the Miller et al. (2021) fit. The Miller et al. (2021) fit was obtained for a capillary

electrospray at a lower flow rate ($Q = 0.40\ nL/s$) than our data, which may partially explain why the error is higher for that fit compared to the Gamero-Castaño et al. (2021) fit. We also note that mass flow rate obtained for the zero energy deficit case ($\Delta E = 0$) is also quite close to the reference value, $\dot{m}_{Ref}$, suggesting that reasonable results can be obtained from time-of-flight data simply by assuming $V_B \approx V_{em}$. However, as mentioned previously, the true energy distribution in a capillary electrospray beam is clearly not constant. It is unclear how the assumption that $V_B \approx V_{em}$ will affect time-of-flight results at a different beam current, and we believe it is better practice to use experimental fits for $V_B(m/q)$.

Table 2: Thrust and Mass Flow Rates obtained from time-of-flight data assuming different values for the beam potential V_B. The large energy spread in capillary electrospray beams causes significant errors when evaluating Eqn. 2 and Eqn. 3 using a constant V_B. *Gamero-Castaño et al. (2021), ** Miller et al. (2021).

Assumed Energy Deficit	V_B (V)	Thrust (μN)	Mass Flow Rate (μg/s)	Volume Flow Rate (nL/s)
$\Delta E = 0\ V$	2000	1.22	1.12	0.738
$\Delta E = 230\ V$	1770	1.08	0.993	0.653
ΔE from [9]	$f(m/q)^*$	1.16	1.10	0.726
ΔE from [10]	$f(m/q)^{**}$	1.27	1.21	0.795
Reference Value: Gamero-Castaño (2008):			**1.11**	0.73

V. Conclusion

We have presented the design and validation of a low-cost, low-noise time of flight mass spectrometer (ToF-MS) for electrospray propulsion diagnostics. Based on an early design by Lozano [5], our ToF-MS is inexpensive (~$1,000 to $2,000 USD) and is suitable for studying droplet-heavy electrospray sources, such as capillaries, and for sources operating in the pure-ion regime, such as porous electrospray thrusters. Here, two major improvements have been made to Lozano's original design: (1) improving the electrostatic shielding around the gate and collector to reduce gate-induced noise (section II.C.2), and (2) using a high-performance transimpedance amplifier (Appendix B) connected directly to the ToF collector. Compared to Lozano's design (2003), our system has considerably shorter gate-induced noise duration (260 ns vs. ~4 μs FWHM) despite the compact dimensions of our system ($L_{ToF} = 116\ mm$ vs. $746\ mm$) [5]. At full bandwidth, the gate-induced noise for our ToF-MS is ~4 nA peak and 260 ns FWHM, which settles quickly enough to resolve the fastest ions (~1.5 – 2 μs) without interference from the gate.

The transimpedance amplifier (TIA) used in this work was a low-cost, custom TIA with a transimpedance gain of 10^6 Ω and a noise level of 395 pA rms at 1.4 MHz. Using this TIA, our ToF-MS was used to measure *m/q* distributions in the plume of a single capillary emitter with a beam current of 485 nA. The electrospray source was rotated in 5° increments to measure *m/q* as a function of angle. These angle-resolved data were analyzed (Appendix A) to calculate the total thrust, accounting for cosine losses, and the propellant flow rate. This flow rate was compared against the flow rate inferred from the beam current to validate the ToF-MS and data analysis methods. We found the best agreement between flow rate measurements when treating the beam potential V_B as a function of *m/q*, as suggested by the literature [9,10]. In our case study, the flow rate determined by ToF differed from flow rate inferred from beam current (based on correlations from [11]) by -0.5% and +8.9% for the ΔE fits published by Gamero-Castano et al. (2021) and Miller et al. (2021), respectively. Assuming a constant beam potential of $V_B \approx V_{em}$ also resulted in a low error but is not a realistic assumption and may result in incorrect thrust or flow rate measurements under different conditions. While these results are encouraging, we acknowledge the need to collect data at additional flow rates to provide a more robust validation of our ToF-MS, and to confidently draw conclusions regarding the treatment of beam potential.

We have demonstrated that a low-cost time-of-flight instrument can be built using resources available to most university labs. That instrument can be validated using a simple capillary emitter, inferring propellant flow rate from the beam current based on correlations in the literature. The process described here is inexpensive and relatively simple, providing researchers with a robust and affordable means to study electrospray thrusters and other electrospray sources.

VI. Acknowledgements

This work was supported by a NASA Space Technology Research Fellowship for Christopher Lyne, NASA Grant 80NSSC19K1165, with technical mentor Dr. Thomas Liu.

VII. Appendix

Appendix A: Calculating Thrust and Flow Rate from Angle-Resolved ToF Data

Time-of-flight instruments in the electrospray literature commonly use large-area collectors that sample the entire electrospray beam simultaneously, sometimes called full-beam ToF. This approach maximizes the collector current, but it does not yield any information about the distribution of *m/q* in the electrospray beam. Full-beam ToF data can be analyzed directly using Eqn. 2 and Eqn. 3 to calculate thrust and mass flow rate, respectively.

In this paper, we have taken ToF measurements at various angles from the electrospray plume center axis (i.e., *spatially resolved* measurements). This approach allows the structure of the beam to be studied (e.g., *m/q* distribution as a function of θ) and allows cosine losses to be accounted for in the thrust calculation. In order to calculate the overall thrust and propellant flow rate, we must integrate over all beam angles (0° to ~30° in this case). Since our ToF data are taken at discrete angles, we will approximate these integrals as a summation over all angles for which there is ToF data. In this analysis, we treat each angle as a 'bin' and assign a fraction of the total beam current to each, denoted I_θ, such that $I_B = \sum_\theta I_\theta$. Then, for each angle θ, Eqn. 2 and Eqn. 3 are used to calculate the mass flow rate and thrust by normalizing and scaling the collector current signal to I_θ rather than I_B and making a correction to thrust to account for cosine losses. Finally, the thrust and flow rate contributions are summed over each angle to find the total thrust and propellant flow rate.

Algorithm for Angle-Resolved ToF Data Analysis

The process used to analyze angle-resolved ToF data to yield overall thrust and propellant mass flow rate measurements are as follows:

1. Start with time-dependent collector current measurements at each angle: $I_c(t)$, as well as the average beam current I_B for each $I_c(t)$. Note that when extractor current is negligible $I_B \approx I_{em}$
2. Calculate $f_c(\theta)$, the fraction of the total beam current measured by the collector for each angle θ. That is, $f_c(\theta) = I_c(t) \,/\, I_B$
3. Multiply $f_c(\theta)$ by $\sin(\theta)$ to account for the total collection area associated with θ to yield $F_c(\theta)$
4. Normalize $F_c(\theta)$ to yield $F(\theta)$, the fraction of beam current that corresponds to each angle θ. The total current corresponding to each angle θ is then $I(\theta) = I_B F(\theta)$

$$F(\theta) = \frac{F_c(\theta)}{\sum_\theta F_c(\theta)} \qquad\qquad I_\theta = I_B F(\theta)$$

5. Normalize the collector current $I_c(t)$ by dividing by the current measured by the collector when the gate is fully open $[I_c]_{Gate\ Open}$, yielding $\widetilde{I_c}(t)$, which should have a step height of 1. That is,

$$\widetilde{I_c}(t) = \frac{I_c(t)}{[I_c]_{Gate\ Open}} \qquad\qquad [\widetilde{I_c}]_{Gate\ Open} = 1 \qquad [\widetilde{I_c}]_{Gate\ Closed} = 0$$

6. Calculate mass flow rate at each angle $\dot{m}_\theta$ using the normalized time-of-flight current signal, $\widetilde{I_c}(t)$, scaled by the total current corresponding to that angle, I_θ.

$$\dot{m}_\theta(\theta) = \frac{2}{L^2} I_\theta \int_0^\infty |V_B|\, t^2 \frac{d\widetilde{I_c}(t)}{dt} dt$$

7. Calculate thrust at each angle $T_\theta(\theta)$ using $\widetilde{I_c}(t)$ scaled by I_θ, accounting for cosine losses (losses due to non-axial thrust) by multiplying by $\cos(\theta)$.

$$\dot{T}_\theta(\theta) = \frac{2}{L} \cos(\theta)\, I_\theta \int_0^\infty |V_B|\, t \frac{d\widetilde{I_c}(t)}{dt} dt$$

8. Finally, calculate the overall mass flow rate and thrust T by summing the contributions at each angle θ

$$\dot{m} = \sum_\theta \dot{m}_\theta(\theta) \qquad\qquad T = \sum_\theta T_\theta(\theta)$$

Appendix B: Transimpedance Amplifier Design

Introduction

A transimpedance amplifier (TIA) is an electronic circuit that is used to measure current and is usually implemented with an operational amplifier (op-amp). TIAs are often used with photodiodes and other sensors that behave like current

sources. Like most current-to-voltage converters, the TIA relies on the voltage drop produced by current passing through an impedance (e.g., a resistor in parallel with a capacitor). However, TIAs have a key advantage over a simple current shunt: the bandwidth of a TIA (proportional to the inverse of response time) does not depend on the capacitance of the sensor. This allows a large impedance to be used as the current shunt, yielding a high transimpedance (current-to-voltage) gain, while maintaining a high bandwidth.

Commercial TIAs that are suitable for time-of-flight experiments are available for purchase, such as the DHPCA-100 from FEMTO Messtechnik GmbH. For a less expensive option, TIAs can be fabricated from op-amps and supporting components. This appendix gives a brief background on TIAs, then describes the design and fabrication of the custom-built TIA used in this work.

Reference Documents

Analysis in this section draws from Texas Instrument application reports SNOA942A "Transimpedance Amplifiers (TIA): Choosing the Best Amplifier for the Job" and SBOA122 "Transimpedance Considerations for High-Speed Amplifiers".

TIA Background: TIA Compared to Simple Shunt Resistor

We begin our discussion of the TIA circuit by comparing its response to the simplest current-to-voltage (I/V) converter, a shunt resistor, shown on the right in Figure 8. Both circuits convert the current signal, $I_c(t)$, into an output voltage, V_{out}, equal to the voltage drop across the resistor R_F. The key difference between these circuits is their response time. Consider a step change in collector current from I_c to zero. In the case of the series resistor, the output voltage exponentially falls from $V_{out} = I_c R_F$ to $V_{out} = 0$. Although the step change in I_c occurs instantly, the capacitance C_{in} must discharge through R_F for V_{out} to fall to zero. That is, C_{in} and R_F form a *low pass filter* with a time constant of $\tau = R_F C_{in}$. For example, with $C_{in} = 10\ pF$ and $R_F = 1\ M\Omega$, the time constant for the shunt resistor is $\tau = 10\ \mu s$, much too slow to resolve the flight times of fast ions (a few μs for our time-of-flight system).

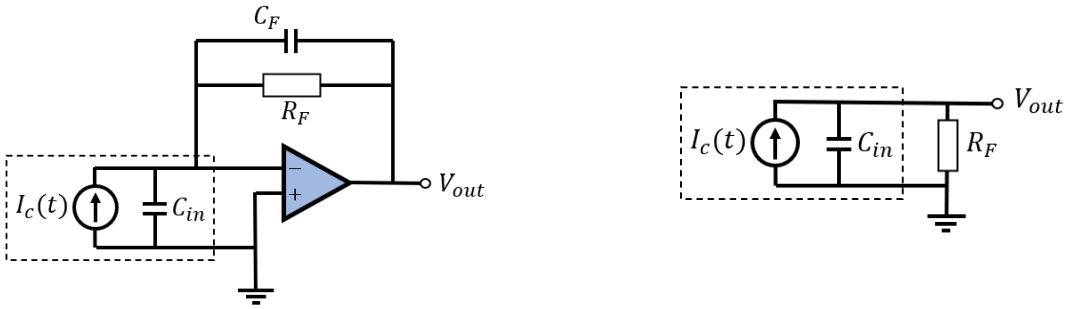

Figure 8: Transimpedance amplifier circuit (left) and shunt resistor circuit (right). The components inside the dashed box are an equivalent circuit model of the time-of-flight collector.

For the transimpedance amplifier (Figure 8 left), the time response can be much faster than the simple shunt resistor because of the gain provided by the op-amp. In an effort to keep its noninverting (+) and inverting (-) inputs at the same voltage, the op-amp will attempt to balance any incoming collector current with an equal current through R_F. That is, the op-amp adjusts V_{out} to make $I_{R_F} = I_c$. This arrangement uses the gain of the op-amp to prevent charge accumulation on C_{in}. An analysis of the TIA time response shows that the TIA is nearly 10^3 times faster than the simple shunt resistor for the conditions considered here.

TIA Background: TIA Stability and Response Time

Recall that op-amp circuits are stabilized by negative feedback. By connecting the op-amp output to its inverting input through a feedback network, the op-amp provides a stable output. However, the total capacitance connected to the inverting input, C_{in}, forms a low pass filter with R_F (see Figure 8) that destabilizes the TIA circuit at high frequencies by introducing a phase shift between the amp output V_{out} and the voltage at the inverting input. At high enough frequencies, this phase shift exceeds 180° and the circuit becomes unstable, causing ringing and an unpredictable output. Physically, this instability is the result of the op-amp not being able to 'keep up' with $I_c(t)$ because it cannot adjust V_{out} quickly enough to force $I_c = I_{R_F}$. Thus, the op-amp is not able to effectively control the voltage at its inverting input and becomes unstable.

In order to stabilize the TIA, we add a feedback capacitor C_F in parallel with the feedback resistor. The feedback capacitor C_F has the effect of limiting the bandwidth of the TIA circuit. To stabilize the TIA, the feedback capacitor should be sized according to Eqn. 5. If the minimum value of C_F is used, the TIA bandwidth (f_{-3dB}) is given by Eqn. 6,

which represents the maximum bandwidth that a TIA can achieve with a given op-amp and C_{in} for a flat (Butterworth) frequency response. Note that the term *GBWP* appearing in Eqn. 5 and Eqn. 6 is a specification of the op-amp, called the *gain-bandwidth product*.

$$C_F \geq \sqrt{\frac{C_{in}}{2\pi(GBWP)R_F}} \quad \text{Eqn. 5}$$

$$f_{-3\,dB} \approx \sqrt{\frac{GBWP}{2\pi R_F C_{in}}} \quad \text{Eqn. 6}$$

As we will see in the next section, the signal-to-noise ratio achieved by a TIA is typically optimized by maximizing R_F and $GBWP$, minimizing C_{in}, and using the lowest bandwidth (f_{-3dB}) that meets the application requirements.

TIA Background: Noise Analysis

A noise analysis of the transimpedance amplifier can be done by calculating an equivalent input-referred noise current, i_{EQ}, as shown in Eqn. 7, taken from the TI Application Report SNOA942A. The input-referred noise current is a useful figure of merit for the TIA, since signal-to-noise ratio can be directly calculated from it as $S/N = I_{signal}/i_{EQ}$. The terms in Eqn. 7 are defined in Table 3. The rightmost column of Table 3 lists the values for the TIA used in this work.

$$i_{EQ} = \sqrt{(i_B)^2 + \frac{4k_B T}{R_F} + \left(\frac{e_N}{R_F}\right)^2 + \frac{(e_N 2\pi f C_{in})^2}{3}} \quad \text{Eqn. 7}$$

Symbol	Description	Value Used
i_B	Inverting input spot current noise	$50\ fA/\sqrt{Hz}\ at\ 1\ MHz$ $500\ fA/\sqrt{Hz}\ at\ 10\ MHz$
k_B	Boltzmann constant	$1.38 * 10^{-23}\ J/K$
R_F	Feedback resistor	$1\ M\Omega$
T	Temperature of the feedback resistor	$293\ K$
e_N	Noninverting input spot voltage noise	$2.5\ nV/\sqrt{Hz}$
C_{in}	Inverting input total capacitance	$10\ pF$
f	Noise integration frequency limit	Various

Table 3: Variables used in Eqn. 7 and their values for the TIA used in this work.

The terms on the right side of Eqn. 7 can be interpreted (from left to right) as the op-amp input current noise, thermal noise due to the feedback resistor, op-amp voltage noise, and a capacitive noise term. The op-amp specifications i_B and e_N can be used as selection criteria to minimize the overall current noise i_{EQ}. For a given op-amp, current noise can be minimized, and therefore signal-to-noise can be maximized, by using the largest value of R_F and the lowest C_{in} possible. From Eqn. 6, we recognize that the gain-bandwidth product of the op-amp should also be as high as possible, since R_F is inversely proportional to $GBWP$ for a fixed bandwidth f_{-3dB}.

Design of TIA Used in This Work

The TIA used in this work was designed to meet the requirements listed in Table 4 while achieving a low input current noise. For our TIA design, we selected the Texas Instruments OPA858 op-amp, which has an exceptionally high gain-bandwidth product of 5.5 GHz and a low input bias current of 10 pA. We paired the OPA858 with a feedback resistor $R_F = 1\ M\Omega$ to achieve a transimpedance gain of $10^6\ \Omega$ (1 V/μA).

Table 4: TIA Design Requirements

Specification	Requirement
Bandwidth (f_{-3dB})	$\geq 5\ MHz$
Transimpedance Gain (R_F)	$1\ M\Omega$
Input Bias Current	$\leq 100\ pA$

Using Eqn. 6 we find that C_{in} must be ~35 pF or lower to achieve the required closed-loop bandwidth of 5 MHz. Since the capacitance of a standard RG-58 coaxial cable is about 80 pF/m, this implies that the cable length between the time-of-flight collector and the TIA must be less than ~45 cm (~18 inches). The collector capacitance, in our case about 6 pF, further reduces the allowable cable length to under 36 cm. We see from Eqn. 7 that reducing C_{in} improves the noise performance of the TIA. In addition, a shorter cable between the collector and TIA reduces electromagnetic interference and gate-induced noise. For these three reasons (higher bandwidth, lower random noise, lower non-random noise), we chose to mount the TIA directly on the time-of-flight current collector, connecting the two via a rigid SMA coaxial connector. We estimate that this arrangement yields a total input capacitance of $C_{in} \approx 10\ pF$. From Eqn. 5 and Eqn. 6 we find that the required feedback capacitance is $C_F \geq 17\ fF$, resulting in a maximum achievable bandwidth of 9.35 MHz.

Performance of TIA Used in This Work

After the TIA was fabricated, a series of tests were performed to verify functionality and to measure its noise characteristics and time response. The TIA has a transimpedance gain of 976 kΩ and a maximum bandwidth of >10 MHz. The measured bandwidth in excess of 10 MHz suggests that C_F is slightly too low, based on Eqn. 5 and Eqn. 6. Figure 9 shows the transimpedance amplifier output voltage in response to a 2 nA square wave. In Figure 9, the oscilloscope lowpass filter was used to limit bandwidth to 1.4 MHz, resulting in a 1% settling time of about 520 ns. Waveform averaging was not used in Figure 9, which would result in a decrease in noise by a factor of $\sqrt{n}$ where n is the number of waveforms averaged.

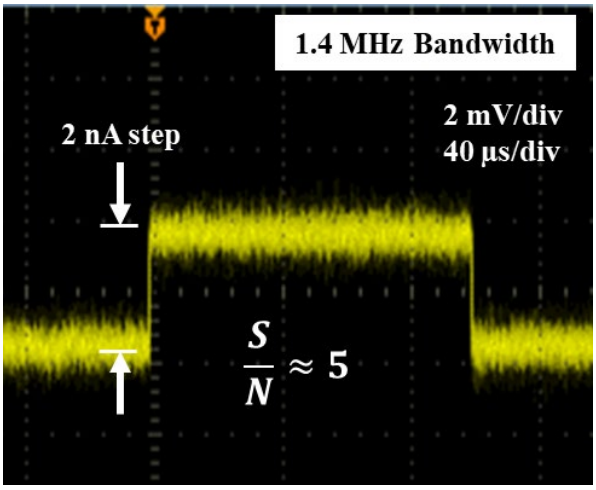

Figure 9: TIA step response to a 2 nA square wave, lowpass filtered to 1.4 MHz. Measured noise was approximately 395 pA rms.

Specification	Custom TIA	DHPCA-100
i_{EQ} *at* ~1 MHz *and* 10^6 Ω	$333\ fA/\sqrt{Hz}$	$140\ fA/\sqrt{Hz}$
Transimpedance Gain	10^6 Ω	10^2 - 10^8 Ω
Approximate Cost	~$150 USD	~$3k - $4k USD

Table 5: Comparison of transimpedance amplifiers: Custom TIA (this work) vs. COTS option, FEMTO DHPCA-100

Table 5 compares the transimpedance amplifier used in this work to a commercial option, the DHPCA-100 by FEMTO Messtechnik GmbH. The commercial option has an input current noise about 2.4 times lower than the TIA used in this work, $140\ fA/\sqrt{Hz}$ at 1.8 MHz compared to $333\ fA/\sqrt{Hz}$ at 1.4 MHz, respectively. The COTS option is also more flexible, since the transimpedance gain can be adjusted with a knob from 10^2 to 10^8 Ω. Nonetheless, we found the performance of the custom TIA to be adequate for our application – it was able to measure sub-nanoamp signals at a bandwidth of >1 MHz, allowing us to measure *m/q* as a function of angle in the plume of a single capillary emitter. When paired with waveform averaging, this custom TIA is able to achieve adequate performance for most electrospray time-of-flight applications, providing a low-cost alternative to commercial transimpedance amplifiers.

Fabrication of TIA Used in This Work

The TIA used in this work uses the OPA858 op-amp from Texas Instruments. Because of the relatively high bandwidth requirement for this TIA (~5 MHz), the TIA circuit must be carefully designed and fabricated to minimize parasitic capacitances and inductances in the circuit. Fortunately, a 'development module' is available from the manufacturer, the OPA858EVM, which features the OPA858 soldered to a professionally-designed printed circuit board with supporting components. The OPA858EVM can be reconfigured into a high-performance transimpedance amplifier with a few simple modifications to the default circuit design.

A user's manual for the OPA858EVM is available from Texas Instruments, document SBOU200. Referring to figure 1 in the user's manual, the following modifications can be made to reproduce the TIA design used in this paper: remove resistors R3 and R7, replace resistor R2 with R=976 kΩ, replace resistor R6 with R=50 Ω. R2 is now the feedback resistor, R_F. The parasitic capacitance of R2 may be sufficient to meet the feedback requirement $C_F \geq 17\ pF$, but our circuit showed considerable peaking at high frequencies that indicated that C_F was too low. We increased C_F by placing a small piece of copper tape of top of R2, which capacitively couples to R2. One end of the copper tape was soldered to the pad of R2 on one side, and a small amount of hot glue was placed between the tape and the resistor R2. The hot glue was then heated, and the tape was adjusted while monitoring the TIA response to a square wave input signal. Once the square wave shape indicated that the circuit was properly compensated, the hot glue was cooled to secure the tape in place. This method allowed us to dynamically adjust C_F based on the TIA response rather than relying on C_F calculated from an estimated C_{in}. Other methods for adding a feedback capacitance to this circuit were not explored in this work. One possible solution might be to replace R2 with two 2 MΩ resistors in parallel (by stacking the surface mount resistors) to achieve the same feedback resistance $R_F = 1\ M\Omega$ with double the parasitic capacitance. Another possible solution is simply to use a higher feedback resistance (e.g., $R_F = 2\ M\Omega$) which requires a lower feedback capacitance to stabilize. Again, these two suggested alternative solutions for adding C_F were not attempted here and would require more analysis to assess their viability.

Fabricating the TIA used in this work requires replacing several surface mount resistors on a pre-configured printed circuit board. The most difficult part of fabricating this TIA is the soldering and desoldering of these resistors, as well as adding C_F, because of their small size. For example, R2 is an 0402 size resistor (1 mm by 0.5 mm) that is in close proximity to the op-amp. These components may be soldered by hand if great care and the right tools are used. For this work, we used a stereo microscope with a magnification of 10x to 45x, a Hakko FX-951 soldering station with FM-2032 micro soldering iron and a variety of soldering tips, and a pair of ESD-safe tweezers with sharp tips.

Once the TIA circuit has been completed (by modifying a OPA858EVM development board), the TIA functionality can be checked by applying a current signal to the negative input terminal of the TIA, via the coaxial connector on the OPA858EVM. Do not exceed any of the absolute maximum specifications listed on the OPA858 data sheet, such as maximum input voltage or maximum supply voltage, or the OPA858 op-amp may be permanently damaged. In this work, the TIA was operated on a supply voltage of ±2.5 V with the positive input not connected (it is grounded on the PCB via R1).

VIII. References

[1] O'reilly, D., Herdrich, G., and Kavanagh, D. F. "Electric Propulsion Methods for Small Satellites: A Review." *Aerospace*, Vol. 8, No. 1, 2021, pp. 1–30. doi:10.3390/aerospace8010022.

[2] Courtney, D. G., Dandavino, S., and Shea, H. "Comparing Direct and Indirect Thrust Measurements from Passively Fed Ionic Electrospray Thrusters." *Journal of Propulsion and Power*, Vol. 32, No. 2, 2016, pp. 392–407. doi:10.2514/1.B35836.

[3] Gamero-Castaño, M. "Characterization of a Six-Emitter Colloid Thruster Using a Torsional Balance." *Journal of Propulsion and Power*, Vol. 20, No. 4, 2004, pp. 736–741. doi:10.2514/1.2470.

[4] Gamero-Castaño, and Hruby, V. "Electrospray as a Source of Nanoparticles for Efficient Colloid Thrusters." *Journal of Propulsion and Power*, Vol. 17, No. 5, 2001, pp. 977–987. doi:10.2514/2.5858.

[5] Lozano, P. C. *Studies on the Ion-Droplet Mixed Regime in Colloid Thrusters*. PhD dissertation, MIT, Department of Aeronautics and Astronautics, 2003. 29, 2003.

[6] Miller, S. W., Prince, B. D., and Bemish, R. J. "Orthogonal Time-of-Flight Mass Spectrometry of an Ion Beam with a Broad Kinetic Energy Profile." *Review of Scientific Instruments*, Vol. 88, No. 10, 2017. doi:10.1063/1.5007879.

[7] Adduci, A. C., Rovey, J. L., Lyne, C. T., Putnam, Z. R., Lembeck, M. F., Ma, C., Ryan, C. N., and Berg, S. P. Characterization of Ionic Liquid Multimode Propellant Operating in a Porous Glass Electrospray Thruster. IEPC-2022-500.

[8] Krejci, D., Mier-Hicks, F., Thomas, R., Haag, T., and Lozano, P. "Emission Characteristics of Passively Fed Electrospray Microthrusters with Propellant Reservoirs." *Journal of Spacecraft and Rockets*, Vol. 54, No. 2, 2017, pp. 447–458. doi:10.2514/1.A33531.

[9] Gamero-Castaño, M., and Cisquella-Serra, A. "Electrosprays of Highly Conducting Liquids: A Study of Droplet and Ion Emission Based on Retarding Potential and Time-of-Flight Spectrometry." *Physical Review Fluids*, Vol. 6, No. 1, 2021, p. 13701. doi:10.1103/PhysRevFluids.6.013701.

[10] Miller, S. W., Ulibarri-Sanchez, J. R., Prince, B. D., and Bemish, R. J. "Capillary Ionic Liquid Electrospray: Beam Compositional Analysis by Orthogonal Time-of-Flight Mass Spectrometry." *Journal of Fluid Mechanics*, Vol. 928, 2021, pp. 1–32. doi:10.1017/jfm.2021.783.

[11] Gamero-Castaño, M. "Characterization of the Electrosprays of 1-Ethyl-3-Methylimidazolium Bis(Trifluoromethylsulfonyl) Imide in Vacuum." *Physics of Fluids*, Vol. 20, No. 3, 2008. doi:10.1063/1.2899658.

[12] Lozano, P. C. "Energy Properties of an EMI-Im Ionic Liquid Ion Source." *Journal of Physics D: Applied Physics*, Vol. 39, No. 1, 2006, pp. 126–134. doi:10.1088/0022-3727/39/1/020.

[13] Gañán-Calvo, A. M., López-Herrera, J. M., Herrada, M. A., Ramos, A., and Montanero, J. M. "Review on the Physics of Electrospray: From Electrokinetics to the Operating Conditions of Single and Coaxial Taylor Cone-Jets, and AC Electrospray." *Journal of Aerosol Science*, Vol. 125, No. May, 2018, pp. 32–56. doi:10.1016/j.jaerosci.2018.05.002.

[14] Lyne, C. T., Rovey, J., and Berg, S. P. Monopropellant-Electrospray Multimode Thruster Testing Results: Electrospray Mode. *AIAA Propulsion and Energy Forum, 2021*. AIAA 2021-3439. https://doi.org/10.2514/6.2021-3439.